

PREMIXED LIFTED HYDROCARBON FLAMES CONTROLLED BY PERIODICAL FORCING

Sergey V. Alekseenko^{1,2}, Vladimir M. Dulin^{1,2}, Yuriy S. Kozorezov¹, Dmitriy M. Markovich^{1,2*}

1: Institute of Thermophysics, Siberian Branch of Russian Academy of Sciences
1 Lavrentyev Avenue, 630090, Novosibirsk, Russia
*email: dmark@itp.nsc.ru

2: Department of Physics, Novosibirsk State University
2 Pirogova Street, 630090, Novosibirsk, Russia

ABSTRACT

The present work is devoted to the experimental study of the axial forcing effect on propane-air and methane-air lifted turbulent flames. The forced flames without swirl and with strong swirl were studied by means of stereo PIV. The spatial distributions of the average velocity and components of turbulent kinetic energy were measured. Dynamics of the large-scale vortices was also investigated by means of high-repetition stereo PIV. For the strongly swirling propane-air flame with vortex breakdown, it was observed that the high-amplitude axial forcing can provide an increase of turbulent combustion rate and suppress vortex core precession near the nozzle exit due to interaction of ring vortices with the flame.

PAPER TITLE AND AUTHOR(S)

The application of a swirl is often used for stabilization of jet flames via increasing turbulent fluctuations upstream the flame front and by providing a low-velocity region or recirculation zone (for low or high swirl rates, respectively) near the burner exit (Cheng, 2006; Legrand et al., 2009; Alekseenko et al. 2011). Thus, the swirl application can be considered as an efficient way to passively control flow structure of jets and flames. However, even for isothermal swirling jets, substantially different flow regimes can be observed, depending on the swirl rate and the manner in which the swirl is applied (e.g., Liang and Maxworthy, 2005). Generally, increasing swirl intensity above a certain critical value leads to a breakdown of the swirling jets' vortex core. The vortex breakdown (VB) has been observed in different states: spiral, bubble, and conical, where the latter two can be either symmetric or asymmetric. Based on the literature, it can be outlined that the flow structure of the strongly swirling jets with bubble-type VB and precession of the vortex core manifests some common features, even for rather different nozzle geometries. Recent studies (Ruith et al. 2003; Liang and Maxworthy, 2005) indicate that precession of the vortex core in a strongly swirling jet is the result of the global helical instability mode $l = 1$ growth in an absolutely unstable jet flow with an initially axisymmetric recirculation zone (RZ), while the RZ appears near the nozzle exit when the swirling jet column becomes centrifugally unstable after sudden expansion of the flow. In an experimental study of an

isothermal swirling free jet at a low Reynolds number ($Re = 1,000$) and various swirl rates, Liang and Maxworthy (2005) showed that after the VB event, strong helical modes $m = +1$ and $+2$ coexisted in the flow and that $m = +1$ had the largest amplitude. The measurements showed that when the RZ appeared, the $m = +1$ oscillation first dominated the inner shear layer between the central RZ and the mean flow and then affected the outer shear layer between the jet and the ambient fluid. For a turbulent strongly swirling jet Cala et al. (2006) showed that 3D spatial structure of coherent vortices corresponded to a couple of secondary helical vortices (one vortex was located inside the RZ and the other outside, in the outer mixing layer) which were induced by the precession of the vortex core. Obviously, the presence of combustion makes the structure of the swirling jets much more complex, because of gas expansion and buoyancy effects (Mourtazin and Cohen, 2007), a combustion-induced VB phenomenon (e.g., Konle et al. 2003), etc. For example, the presence of combustion is known to suppress the vortex core precession in strongly swirling jets and also to affect the precession weakly (Alekseenko et al., 2011).

Another well-known efficient way to control turbulent structure (formation and downstream evolution of vortices) of non-swirling jet flows is the periodical excitation of the initial velocity (e.g., Broze and Hussain, 1996). In particular, the excitation affects stabilization height of a lifted non-swirling flame via altering ring-like vortices developing in the jet shear layer upstream the flame (e.g., Lin et al., 1993). Periodic forcing also can be used to control the development of large-scale vortices and turbulent mixing in weakly (Gallaire et al., 2004) and even in strongly (Alekseenko et al., 2008) swirling isothermal jets. Based on Large Eddy Simulation of a lean swirling flame in a model combustor, Iudiciani and Duwig (2011) have shown that application of periodic forcing with the frequencies below the precession frequency of the vortex core can result in weakening the core precession and consequently shifts RZ and combustion domain upstream the nozzle. On the basis of experimental and numerical data for premixed swirling flame in a model combustor (the swirl rate was about 0.55) Palies et al. (2011) concluded that the swirling flame response to periodic forcing was governed by two main mechanisms: variation of the swirl rate and roll-up

of large-scale vortices. Depending on the forcing frequency, confluence of these mechanisms can result in high or low level of heat release fluctuations. It is also suitable to note here that small flap actuators can be efficiently used to control vortices formation and mixing in a non-swirling jet (Suzuki et al., 2004) and weakly swirling jet (Saiki et al., 2011). In particular, the actuators can be also utilized to control stabilization of a lifted diffusion flame (Kurimoto et al., 2005).

The present paper aims on the experimental study of rich strongly swirling lifted flames under high-amplitude forcing of the initial velocity to promote ring-like vortices generation. The modification of turbulent reacting and isothermal flows (at the same inflow conditions) was investigated by means of stereo Particle Image Velocimetry (PIV). CH* chemiluminescence imaging was also applied to visualize region of turbulent combustion for the reacting cases.

EXPERIMENTAL SETUP AND APPARATUS

The measurements were performed in a combustion rig consisted of a burner, air fan, plenum chamber, flow seeding device, premixing chamber and section for the air and fuel (propane) flowrate control. The experiments were performed at atmospheric pressure. The burner represented a contraction nozzle with the exit diameter $d = 15$ mm. For the flow swirling, a swirler (with swirl rate $S = 1.0$, estimated from geometrical parameters) was mounted inside the nozzle. It produced a strongly swirling jet flow with a pronounced VB and bubble-type RZ (Alekseenko et al., 2008, 2011). During the present PIV study of the reacting and isothermal flows, Re_{air} number (based on the nozzle exit diameter d , mean flowrate velocity and viscosity of the air) was fixed as 4,100. The equivalence ratio Φ of fuel-air mixture issuing from the burner was 2.5. For the external periodical forcing of the flow, a system consisting of four loud speakers (a similar system was used by Broze and Hussain, 1996), connected to an amplifier, function generator and electric power meter, was used. The normalized (by nozzle exit diameter d and the mean flowrate velocity U_0 of the mixture) forcing frequency, i.e., the Strouhal number St , was varied from 0.1 to 3. The forcing amplitude was calibrated by a Laser Doppler Velocimetry probe for various frequencies and ac power of sine voltage applied to the system of loud speakers. The referred amplitude of forcing a_f was defined as the intensity of the longitudinal velocity fluctuations at exit of the nozzle without swirler.

For the instantaneous velocity measurements, a "PIV-IT" Stereo PIV system consisted of a double-cavity 70 mJ Nd:YAG pulsed laser, couple of 4M CCD cameras and a synchronizing processor was used. Additionally, a high-repetition Stereo PIV system, assembled of a Pegasus PIV Nd:YLF double-cavity laser (2×10 mJ at $2 \times 1,000$ Hz) and couple of PCO 1200hs CMOS cameras (636 fps at full resolution 1280×1024 pix), was utilized to investigate dynamics of large-scale vortices. In both cases the laser sheet formed by the system of lenses had a minimal thickness of 0.8 mm in the measurement section. In order to provide PIV measurements, the main flow issuing from the nozzle was seeded by TiO_2 particles with the average diameter of 1 μm .

The ambient air was seeded by a fog generator. The cameras were equipped with narrow-bandwidth optical filters admitting the emission of the laser and suppressing the radiation of the flame. The captured PIV images were processed by an iterative cross-correlation algorithm with an image deformation, a final interrogation area size of 32×32 pixels, and 50% overlap. Due to a non-uniform seeding of the tracer particles on the flow, the modified cross-correlation algorithm (Alekseenko et al., 2011) was used to account for the number of particles present in each interrogation area. Calculated instantaneous velocity vectors were also validated and "false" vectors were removed. Stereo calibration was performed by using a multi-level calibration target and a 3rd-order polynomial transform. In addition, to minimize the stereo calibration error, an iterative correction procedure of possible misalignment of the laser sheet and target plane was applied. All PIV measurements were performed in a central plane of the jet/flame. For each regime, 1,500 and 2,400 instantaneous three-component velocity fields were measured by conventional PIV and high-repetition PIV systems, respectively. In the latter case, four independent sets of 600 image pairs were captured with the acquisition frequency of about 800 Hz. Based on the estimated instantaneous velocity fields, the spatial distributions of the mean velocity and components of turbulent kinetic energy (TKE) were calculated. To investigate the spatial structure of large-scale vortices emerging in the studied flows, a second-order centered difference scheme was used to calculate instantaneous vorticity fields. It should be mentioned that the scheme used is a low-pass derivative filter with a transfer function similar to that of the cross-correlation operator in the case of a 50% interrogation area overlap. Thus, the shown below distributions of the instantaneous vorticity and velocity correspond only to large-scale fluctuations (greater than 1.1 and 2.1 mm for the cases of conventional PIV and high-repetition PIV, respectively).

For the analysis of the spatial domain of turbulent combustion, CH* chemiluminescence signal from the swirling flames was captured by an UV-sensitive 1.5 Mpix ICCD camera equipped with a band-pass optical filter (430 ± 5 nm). To allow comparison between the unforced and forced cases, the exposure duration (100 μs) and aperture of the lens (set to the smallest value) were fixed. The chemiluminescence of other radicals admitted by the filter was assumed to be small, at least for the flame front. Five hundred 10-bit images of CH* chemiluminescence were captured, converted to floating point data, and then averaged for each combustion regime. For analysis of the spatial structure of turbulent combustion region, an inverse discrete Abel transform (A^{-1}) was applied to the averaged images.

RESULTS

Combustion regimes

The present section focuses on combustion regimes of the propane-air flames, since spatial structure of the methane-air flames was similar. Figure 1 shows a $Re-\Phi$ diagram with the regions of typical combustion regimes and a blow-off curve

for the non-swirling ($S = 0$) propane-air flame. In general, the domain between the blow-off and flash-back limits in the $Re-\Phi$ diagram can be divided into three main regions: an attached (seated) Bunsen flame, lifted (suspended) flame and the third region, where the lifted or attached flame regime could be realized depending on the manner in which the flame was ignited. For the methane-air flame, $Re-\Phi$ domain of stable lifted flames was found to be smaller. Figure 1 demonstrates that the lift-off limits for propane and methane attached flames were rather similar. This agrees well the early result by Lewis and von Elbe (1943) that the lift-off limit is defined by velocity gradient at the inner wall of the burner.

Figure 2 shows a $Re-\Phi$ diagram with the regions of typical combustion regimes and a blow-off curve for the strongly swirling ($S = 1.0$) propane-air flame. The domain between the blow-off and flash-back limits in the $Re-\Phi$ diagram can be divided into three main regions of typical combustion regimes: attached flames with the front anchored to the nozzle rim; quasi-tubular flames with the front penetrating inside the nozzle; and lifted flames, which were typical for high Re_{air} and rich mixtures. In general, the strongly swirling turbulent (for Re_{air} typically above 2 000) propane-air or methane-air flames were stabilized inside the recirculation zone (as the quasi-tubular regime) when Φ was in the range close to flammability limits for a homogenous fuel-air mixture at normal conditions (e.g., $0.6 < \Phi < 2.3$ and $0.5 < \Phi < 1.6$ at $Re_{air} = 4\ 000$ for propane and methane, respectively). If Φ was smaller, the flame was blown away; if Φ was higher, the combustion occurred as the lifted flame after the mixing of the main flow, issuing from the nozzle, with the ambient air.

Figures 3a and c show the direct images, as well as the averaged images of integral CH^* chemiluminescence (on the line-of-sight through the flame) for the lifted propane-air flames without swirl ($S = 0$) and with strong swirl ($S = 1.0$), respectively. The chemiluminescence images are presented in pseudo color. In this work we focus on effect of the strong forcing on these two types of lifted flames. The non-swirling lifted flame represented a turbulent combustion domain localized after $z/d = 1.3$ downstream the nozzle exit. Also, since the mixture coming from the nozzle was relatively rich ($\Phi = 2.5$) an extensive region of products afterburning was present further downstream, where soot luminescence was observed. For the strongly swirling lifted flame, the domain of intensive turbulent combustion was significantly wider and located closer to the nozzle exit (less than one d). Also, products afterburning and soot luminosity can be seen downstream the domain. Figures 3b and d demonstrate the effect of the axial forcing on the non-swirling and strongly swirling lifted flames, respectively. The considered forcing frequency 170 Hz corresponds to the Strouhal number of $St = 0.6$ which is in the range of prevailing frequencies for an isothermal jet "column". The results are presented for a quite large amplitude of the forcing, viz., a_f was 30% of U_0 . For the non-swirling case, the strong forcing resulted in a widening and extension of the combustion domain, but didn't affect the flame stabilization height. It also insignificantly affected the blow-off limit of the lifted propane-air flame (however, for the

methane-air mixture the forcing slightly increased the range of Re and Φ for the stable lifted flames). For the case of the strongly swirling propane-air flame, a considerable modification of the combustion regime was observed for forcing amplitude a_f above 25% of U_0 . In particular, the shown case for 30% demonstrates a less soot luminosity downstream of the domain of turbulent combustion. Analysis of the mean chemiluminescence distributions reveals that the high amplitude periodic forcing led to an increase in overall combustion intensity in the initial region of the lifted flame. The domain of turbulent combustion also slightly moved downstream and became wider. Remarkable, that for the strongly swirling methane lifted flame this effect was not so pronounced (cf. Figures 6c and d).

Non-swirling lifted flame

The spatial distributions of the normalized mean velocity and radial component of TKE for the non-swirling propane lifted unforced and forced ($St = 0.6$ $a_f = 0.3U_0$) flames are shown in Figure 4. Iso-levels of the reconstructed average CH^* chemiluminescence source are also depicted to demonstrate spatial structure of the turbulent combustion domain. In both cases, fluid expansion took place after onset of the combustion domain ($z/d = 1.3$). From the radial component of TKE it can be seen that the forcing dramatically increased the velocity fluctuations in the mixing layer due to promotion of ring-like vortices. Thus, the forcing resulted in an intensification of turbulent combustion after $z/d = 1.3$ and shifting the flame base towards greater radii (viz., from $r/d = 0.67$ to 0.9) due to more intensive mixing of the fuel and ambient air. Nevertheless, the forcing with 170 Hz didn't affect significantly the stability (viz., blow-off limit of stabilisation height) of the lifted propane flame, unlike forcing with 300 Hz (not discussed in the paper).

Strongly swirling lifted flame

Figure 5 shows the forcing effect on the spatial distributions of the mean velocity and radial component of TKE for the lifted turbulent propane-air flame with strong swirl. A bubble-type VB took place both for the unforced and forced cases, and the main flow issued from the nozzle occurred as an annular jet with a certain opening angle. The flow propagated around the RZ located at the jet axis (shown by a red heavy line in Figures 5a and b). A decrease of RZ longitudinal size by the forcing can be seen, while its lateral size was almost constant (around $0.65d$). Also, the intensive combustion domain slightly shifted downstream and became wider when the forcing was applied. In this domain, an increase of the gas velocity magnitude and growth of the jet spreading rate occurred. Besides, the fluid expansion was found to be greater for the forced flame due to an intensification of combustion near the burner exit. A significant modification in distributions of the radial component of TKE by the forcing can be outlined from Figures 5c and d. For the forced case, $\langle v^2 \rangle$ significantly decreased around the jet axis in the vicinity the nozzle exit ($r/d < 0.5$ and $z/d < 0.5$). Similar changes in the distributions

of the azimuthal TKE component were detected (not shown in the paper). This indicates that the precession of the flow inside the RZ was suppressed when the forcing with $St = 0.6$ and $a_f = 30\%$ was applied. Pronounced suppression of vortex core precession took place for the propane-air flame case only, while for the isothermal flow and for the methane-air flame at the same conditions this effect was much smaller (cf. Figures 6a and b). Figure 6 shows the instantaneous velocity and vorticity fields captured by the high-repetition PIV system with the time separation of 1.3 ms. This delay is more than 4.5 times smaller than the forcing period and is expected to be about 3 times lesser than interval of the vortex core precession. In general, for the unforced cases (only isothermal unforced flow is shown in Figure 6) the instantaneous flow pattern of coherent vortex structures appeared to be rather similar. The large-scale vortices were formed both in the inner and outer shear layers of the annular flow. It is expected that each shear layer was dominated by one most powerful helical vortex, induced near the stagnation point of the RZ, when the wriggling reverse flow faced the main flow issuing from the nozzle. Figures 6b and c show the instantaneous velocity and vorticity fields for the forced ($St = 0.6$, $a_f = 30\%$) isothermal jet and methane-air flame, respectively. These examples demonstrate that the high amplitude forcing induced nearly-symmetrical couples of positive and negative vortices both in the outer and inner mixing layer, while the reverse flow still wriggled inside the RZ due to the core precession. Taking into account the relatively large amplitude of the forcing, these couples of the opposite vortices are expected to correspond to vortex rings formed in the inner and outer shear layers due to pulsing of the annular flow. From the examples for the forced propane-air flame (Figure 6d), the formation of similar vortex couples can be seen. The main difference from the previous forced cases is that the radial velocity fluctuations inside the RZ for $z/d < 1.0$ were rather small for the forced propane-air flame. Thus, the suppression of the reverse flow precession is expected to occur due to the ring-like vortices interaction with the lifted flame front. It is also supposed, that possible variation of the swirl rate due to the forcing (Palies et al., 2011), had a minor effect in this case, since the swirl rate of the nozzle significantly exceeded a critical value for the VB.

CONCLUSIONS

The flow structure of a non-swirling and strongly swirling lifted propane-air and methane-air turbulent flames under periodical forcing was studied experimentally. Ensembles of the instantaneous velocity fields were measured by means of stereo PIV, and the domain of intensive turbulent combustion was visualized via CH^* chemiluminescence. For the non-swirling propane-air lifted flames the forcing with $St = 0.6$ dramatically increased turbulent fluctuations in the mixing layer and intensified turbulent combustion after the flame onset, but had a weak effect on the stabilization height and blow-off limit. For the strongly swirling lifted flames with bubble-type vortex breakdown, obtained results demonstrate that the strong axial forcing (with amplitude 30% of U_0) can provide an increase of combustion rate for the propane flame

and suppress precession of the vortex core near the nozzle exit due to interaction of the ring-like vortices with the flame. It was observed that these effects were significant only for the case of propane-air flames.

Acknowledgements

The work was supported by Russian Foundation for Basic Research (grants NN 11-08-00985, 11-08-01063).

REFERENCES

- Alekseenko, S.V., Dulin, V.M., Kozorezov, Yu.S., and Markovich, D.M., 2008, "Effect of axisymmetric forcing on structure of a swirling turbulent jet", *Int. J. Heat and Fluid Flow*, Vol. 29, pp. 1699-1715.
- Alekseenko, S.V., Dulin, V.M., Kozorezov, Yu.S., Markovich, D.M., Shtork, S.I., and Tokarev, M.P., 2011, "Flow structure of swirling turbulent propane flames", *Flow, Turb. and Comb.* DOI 10.1007/s10494-011-9340-5.
- Broze, G., and Hussain, F., 1996, "Transitions to chaos in a forced jet: intermittency, tangent bifurcations and hysteresis", *J. Fluid Mech.*, Vol. 311, pp. 37-71.
- Cala, C.E., Fernandes, E.C., Heitor, M.V., and Shtork, S.I., 2006, "Coherent structures in unsteady swirling jet flow", *Exp. Fluids*, Vol. 40, pp. 267-276.
- Cheng, R.K., 2006, "Low Swirl Combustion" *The Gas Turbine Handbook*
- Gallaire, F., Rott, S., and Chomaz, J.-M., 2004, "Experimental study of a free and forced swirling jet", *Phys. Fluids*, Vol. 16, pp. 2907-2917.
- Iudiciani, P., and Duwig, C., 2011, "Large eddy simulation of the sensitivity of vortex breakdown and flame stabilisation to axial forcing", *Flow, Turb. and Comb.*, Vol. 86, pp. 639-666.
- Konle, M., Kiesewetter, F., and Sattelmayer, T., 2008, "Simultaneous high repetition rate PIV-LIF-measurements of CIVB driven flashback", *Exp. Fluids*, Vol. 44, pp. 529-538.
- Kurimoto, N., Suzuki, Y., and Kasagi, N., 2005, "Active control of lifted diffusion flames with arrayed micro actuators" *Exp. Fluids*, Vol. 39, pp. 995-1008.
- Legrand, M., Nogueira, J., Lecuona, A., Nauri, S., and Rodríguez, P.A., 2009, "Atmospheric low swirl burner flow characterization with Stereo-PIV" *Exp. Fluids*, Vol. 48, pp. 901-913.
- Lewis B., and von Elbe, G., 1943 "Stability and structure of burner flames" *J. Chem. Phys.* Vol. 11, pp. 75-97.
- Liang, H., and Maxworthy, T., 2005, "An experimental investigation of swirling jets", *J. Fluid Mech.*, Vol. 525, pp. 115-159.
- Lin, C.K., Jeng, M.S., and Chao, Y.C., 1993, "The stabilization mechanism of the lifted jet diffusion flame in the hysteresis region" *Exp. Fluids*, Vol. 14, pp. 353-365.
- Mourtazin, D., and Cohen, J., 2007, "The effect of buoyancy on vortex breakdown in a swirling jet" *J. of Fluid Mech.*, Vol. 571, pp. 177-189.
- Palies, P., Schuller, T., Durox, D., Gicquel, L.Y.M., and Candel, S., 2011, "Acoustically perturbed turbulent premixed swirling flames", *Phys. Fluids*, Vol. 23, 037101
- Ruith, M.R., Chen, P., Meiburg, E., and Maxworthy T., 2003, "Three-dimensional vortex breakdown in swirling jets and wakes: direct numerical simulation", *J. Fluid Mech.*, Vol. 486, pp. 331-378.
- Saiki, Y., Suzuki, Y., and Kasagi, N., 2011, "Active control of swirling coaxial jet mixing with manipulation of large-scale vortical structures" *Flow, Turb. and Comb.* DOI 10.1007/s10494-010-9274-3.
- Suzuki, H., Kasagi, N., and Suzuki, Y., 2004 "Active control of an axisymmetric jet with distributed electromagnetic flap actuators" *Exp. Fluids*, Vol. 36, pp. 489-509.

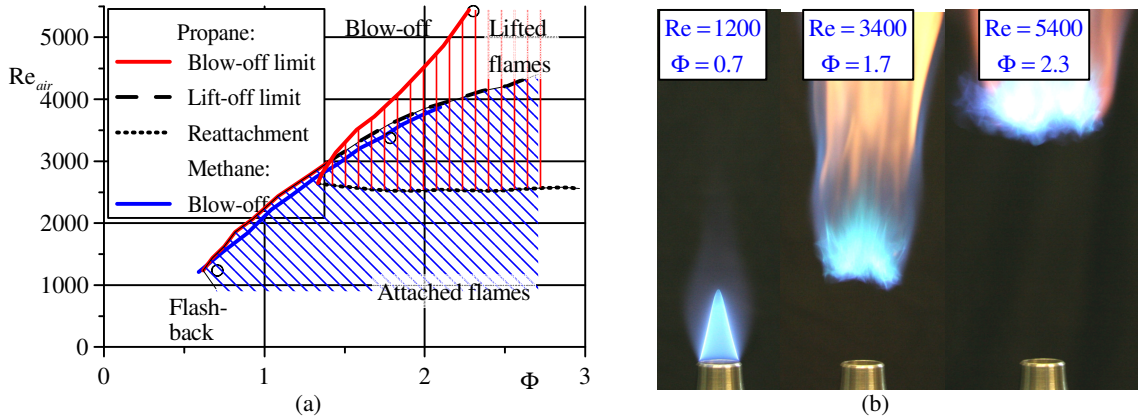


Figure 1. (a) Re_{air} - Φ diagram with typical combustion regimes and blow-off limit for a non-swirling propane-air flame ($S = 0$). \square - attached (seated) flames \square - lifted (suspended) flames. (b) Direct images of typical combustion regimes. Blue solid line shows blow-off limit for a methane-air flame.

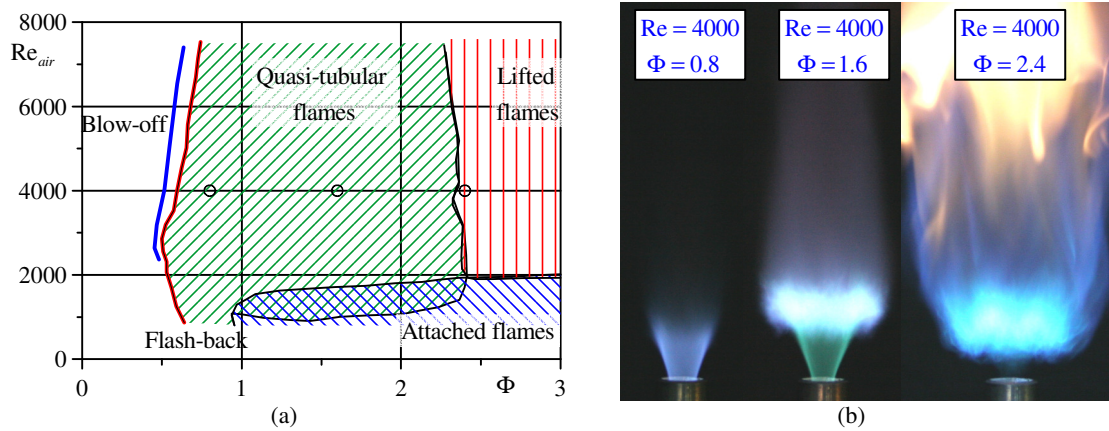


Figure 2. (a) Re - Φ diagram with typical combustion regimes and blow-off limit for a strongly swirling propane-air flame ($S = 1.0$). \square - flames attached to nozzle rim; \square - quasi-tubular flames inside the recirculation zone; \square - lifted flames. (b) Direct images of typical combustion regimes. Blue solid line shows blow-off limit for a methane-air flame.

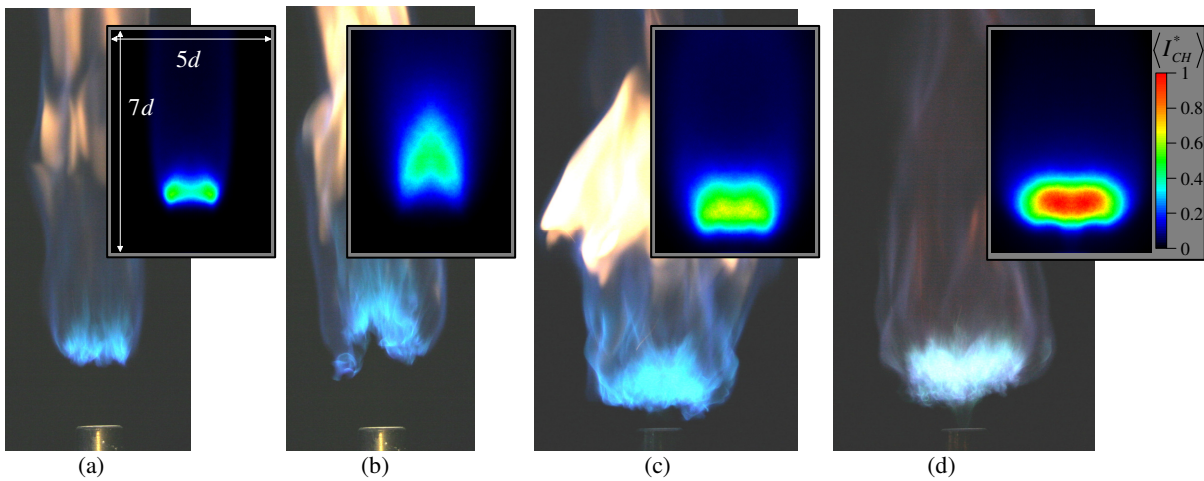


Figure 3. Direct images and mean CH^* chemiluminescence signal for lifted propane-air flames (a, c) without periodic forcing and (b, d) under forcing with $St = 0.6$ and $a_f/U_0 = 30\%$. $Re_{air} = 4\ 100$, $\Phi = 2.5$, $U_0 = 4.7$ m/s. (a, b) no swirl $S = 0$; (c, d) strong swirl $S = 1.0$

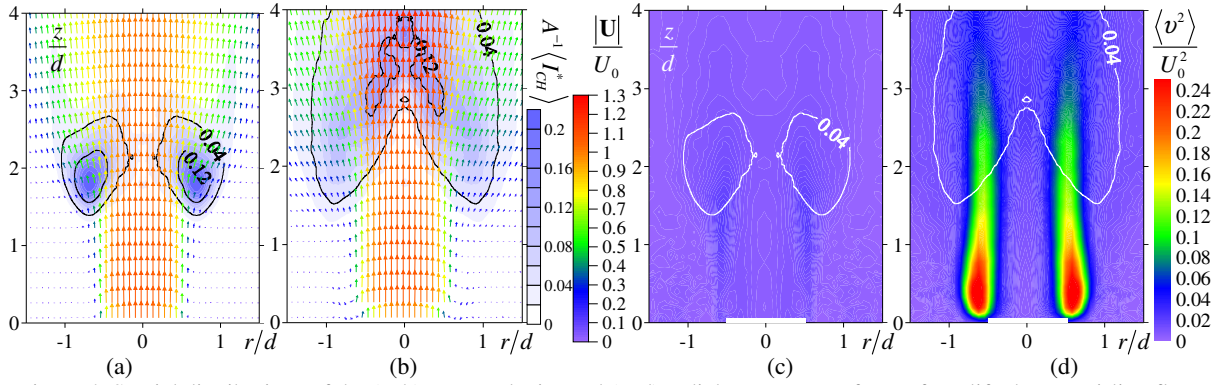


Figure 4. Spatial distributions of the (a, b) mean velocity and (c, d) radial component of TKE for a lifted non-swirling flame (a, c) without periodic forcing and (b, d) under forcing with $St = 0.6$ and $a_f/U_0 = 30\%$. $S = 0$, $Re_{air} = 4\ 100$, $\Phi = 2.5$, $U_0 = 4.7$ m/s. Iso-levels correspond to reconstructed CH^* chemiluminescence source $A^{-1}\langle I_{CH}^* \rangle$

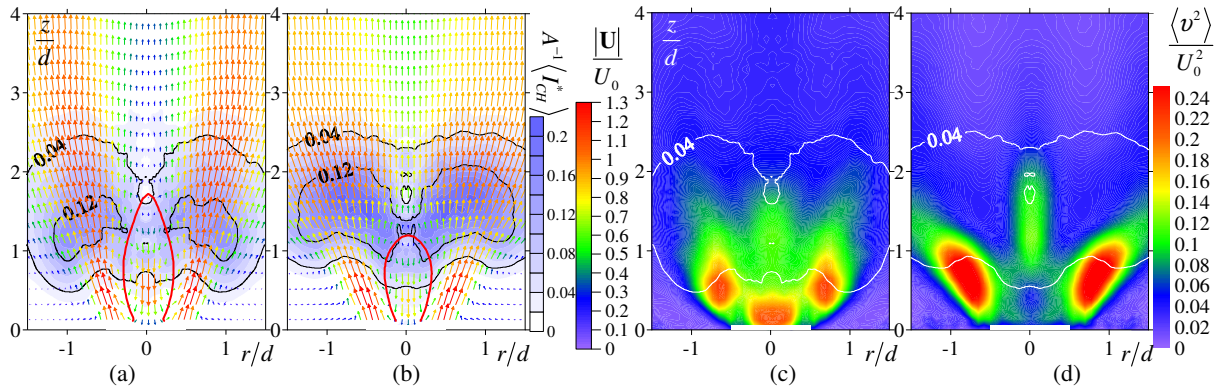


Figure 5. Spatial distributions of the (a, b) mean velocity and (c, d) radial component of TKE for a lifted non-swirling flame (a, c) without periodic forcing and (b, d) under forcing with $St = 0.6$ and $a_f/U_0 = 30\%$. $S = 1.0$, $Re_{air} = 4\ 100$, $\Phi = 2.5$, $U_0 = 4.7$ m/s. Red heavy line shows recirculation zone. Iso-levels correspond to $A^{-1}\langle I_{CH}^* \rangle$

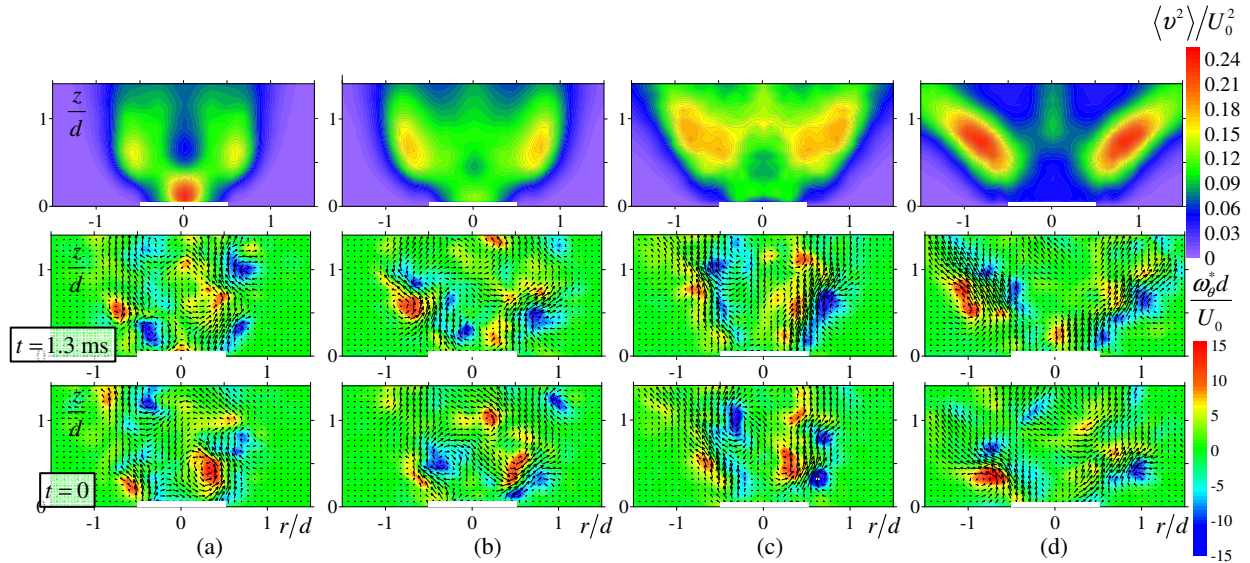


Figure 6. Spatial distributions of the (bottom and middle) instantaneous velocity and vorticity fields and (top) radial component of TKE for strongly swirling jets and lifted flames. $S = 1.0$, $Re_{air} = 4\ 100$, $\Phi = 2.5$, $U_0 = 4.7$ m/s. (a) forced isothermal jet; forced with $St = 0.6$ and $a_f/U_0 = 30\%$ (b) isothermal jet, (c) methane-air flame and (d) propane-air flame.